Article

Cold Spray of Nickel-Based Alloy Coating on Cast Iron for Restoration and Surface Enhancement

Adrian Wei-Yee Tan [1,2,3], Nataniel Yong Syn Tham [2,4], Yao Shian Chua [2], Kaiqiang Wu [1,2], Wen Sun [1,2], Erjia Liu [1,2], Sung Chyn Tan [5] and Wei Zhou [1,2,*]

1   Rolls-Royce@NTU Corporate Laboratory, Nanyang Technological University, 65 Nanyang Drive, Singapore 637460, Singapore; adrian.tan@soton.ac.uk (A.W.-Y.T.); kaiqiang001@e.ntu.edu.sg (K.W.); sunw0013@e.ntu.edu.sg (W.S.); mejliu@ntu.edu.sg (E.L.)
2   School of Mechanical and Aerospace Engineering, Nanyang Technological University, 50 Nanyang Avenue, Singapore 639798, Singapore; nataniel_tham@artc.a-star.edu.sg (N.Y.S.T.); ychua029@e.ntu.edu.sg (Y.S.C.)
3   School of Engineering, University of Southampton Malaysia, Iskandar Puteri 79100, Malaysia
4   Advanced Remanufacturing and Technology Center (ARTC), 3 Cleantech Loop, Singapore 637143, Singapore
5   Rolls-Royce Singapore Pte. Ltd., 1 Seletar Aerospace Crescent, Singapore 797575, Singapore; sungchyn.tan@rolls-royce.com
*   Correspondence: wzhou@cantab.net or mwzhou@ntu.edu.sg; Tel.: +65-6790-4700

Abstract: Cold spray is an emerging additive manufacturing process that allows particles to be coated onto the surface of a base material without melting. It is suitable to repair components made from temperature-sensitive materials, such as grey cast iron, which cannot be easily restored using conventional methods like welding or thermal spray. In this study, the nickel-based alloy Inconel 625 was successfully coated onto a grey cast iron (GJL250) using a cold spray process, and extensive experiments were carried out to study the effects of diffusion between the coating and the substrate after heat treatment at 400, 600, 850 and 1050 °C for 3 and 6 hours durations. The coatings in all conditions were dense (0.25% to 3%) and had defect-free interfaces. Under heat treatment, the diffusion layer increased in thickness with increasing temperature and duration due to atomic diffusion. The Inconel 625 coating is also shown to be effective against oxide growth as compared to grey cast iron. The hardness of the coatings is also stable at high temperatures. The heat-treated coatings at 600 °C achieved a peak hardness of around 500 HV, which is 30% and 60% higher than the as-sprayed coating and grey cast iron substrate, respectively, because of the possible formation of recrystallized nanostructured grains and strengthening precipitates. These findings demonstrate the potential application of using cold spray on nickel-based alloy coatings for restoration and surface enhancement of grey cast iron components, such as engine blocks and pump housings.

Keywords: cold spray; additive manufacturing; Inconel 625; Diamalloy 1005; coating; cast iron; heat treatment; hardness

1. Introduction

Grey cast iron is the most common cast iron and widely used cast material based on weight. It offers a good combination of strength, abrasion resistance and damping capacity, but is still easy to machine and can be finished to a high standard. Grey cast iron is used for a variety of applications, such as combustion engine cylinder blocks, pump housings, valve bodies, and machine tool mountings [1–3]. However, it is often subjected to oxidation, wear, and tear, leading to detrimental properties over time and subsequent replacement of the entire part.

Nickel-based alloys, such as Inconel 625 (IN625), have excellent high-temperature oxidation and good corrosion resistance [4–6], and can be used to repair and protect grey cast iron components from degradation, increasing the life span of the part. However, grey cast iron has been a challenging material to repair through conventional high-temperature methods due to its high carbon content (2.5% to 4%) and the flake morphology of graphite [7].

Welding of grey cast iron would promote the growth of hard and brittle microstructures (martensite, ledeburite, and iron carbides [8,9]), inducing thermal stress and large heat affected zones (HAZ), making it susceptible to cracking. On the other hand, repair using thermal spraying, such as plasma spraying, flame spraying, and high-velocity oxygen fuel (HVOF) spraying, has a relatively low adhesion strength to the substrate with mechanical bonding [10].

Cold spray is an alternative technique to deposit IN625 onto grey cast iron for repair purposes. It is a low-temperature additive manufacturing process where particles are accelerated to supersonic speeds and impact on the target substrate surface to form a deposit or coating. The particles remain in their solid-state condition throughout the process since the bonding mechanisms are a possible combination of adiabatic shear instability [11], pressure-driven hydrodynamic jetting [12], and mechanical interlocking [13]. The detailed working principles of the cold spray process have been widely reported in the literature [14–27]. Several advantages of the cold spraying IN625 coating onto grey cast iron include minimal phase change, oxidation, and residual stresses. These conditions would allow the bonding of dissimilar materials, such as IN625 and grey cast iron.

There have been only two published papers so far reporting the cold spray of coatings on grey cast iron, to the best of the authors' knowledge [19,20]. Champagne and Helfritch [28] and Tham et al. [29] demonstrated that nickel alloy could be cold sprayed on grey cast iron components for restoration, but no in-depth coating analyses were reported. Nevertheless, recent studies have demonstrated that IN625 coatings are capable of being cold sprayed [30–33], which highlighted the effectiveness of these coatings for surface enhancement and repair. Sun et al. [30] successfully deposited IN625 coatings on IN718 substrates via a high-pressure cold spray process. The porosity level of the coatings was around $2.41\% \pm 0.3\%$ with limited irregular micropores, the adhesion strength was more than 68 MPa and the interparticle cohesive strength was around 307 ± 15 MPa. Chaudhuri et al. [31] conducted an extensive microstructural investigation of cold sprayed IN625 on low alloyed steel. It is reported that due to severe deformation of the particles (from the high-speed impact on a substrate), significant strain accumulation happened within the coating, which resulted in a decrease in the average IN625 crystallite size from 240 to 160 nm. The substrate region close to the coating-substrate interface, showed a 2 μm thin layer of heavy grain refinement with an average grain size of 250 nm. In the study by Wu et al. [34], surface enhancement of Al alloy by cold sprayed IN625 was investigated. The substantial hardness increment of IN625 coating compared with wrought material leads to significantly better wear resistance. Heat treatment (HT) studies of cold sprayed IN625 on grey cast iron are required for the repaired components used for high-temperature operations. However, such studies have not been reported except for the preliminary study by Tham et al. [29].

Based on these research gaps, this work focuses on studying the feasibility of cold spraying IN625 coating onto grey cast iron substrates, which could enable the repair/restoration/enhancement of grey cast iron components. The samples will be heat-treated at different temperatures and durations, and evaluated in terms of microstructure evolution, interface diffusion, effectiveness in reducing oxidation growth, and changes in mechanical properties.

2. Materials and Methods

2.1. Materials and Coating Deposition

The feedstock powder used was Diamalloy 1005 (which is hereafter referred to as IN625 due to its similarity to IN625), a gas-atomised nickel-based superalloy powder (Oerlikon Metco, Pfäffikon, Switzerland). The powder is spherical in shape, with a particle size range of 11 to 45 μm. This material has excellent oxidation and corrosion resistance at elevated temperatures, which makes it suitable as an overlay coating for less noble materials like grey cast iron [4]. Grey cast iron (GJL 250) plate is used as the substrate due to the target application. The dimensions of the plate (L × W × T) are 400 mm × 50 mm × 20 mm. It is a type of lamellar cast iron that has a graphite-flake structure [2]. The substrate is

sand blasted before cold spraying. The material properties and chemical compositions of the powder and substrate are shown in Tables 1 and 2, respectively. A stainless-steel-based bond coat powder, DYC-8 (Dycomet Europe, Akkrum, The Netherlands), was also deposited to create a graphite-flake free zone that can ensure strong adhesion between the IN625 coating and a grey cast iron substrate, and its composition is discussed in Section 3.1 (Cross-section analysis).

Table 1. Material properties of the powder and substrate.

Nomenclature	Unit	Diamalloy 1005 (IN625) Powder [35,36]	Grey Cast Iron (GJL250) Substrate [37]
Density	kg/m^3	8440	7200
Young's Modulus	GPa	207	103–118
Tensile strength	MPa	930	250–300
Melting point	°C	1290–1350	1127–1204
Thermal conductivity	W/m·K	9.8	50
Specific heat	J/kg·K	410	460
Thermal expansion coefficient	μstrain/K	12.8	10–13

Table 2. Chemical compositions of the powder and substrate.

Materials	Ref.	Elements (wt.%)					
Diamalloy 1005 (IN625) Powder	[4]	**Ni**	**Cr**	**Mo**	**Fe**	**Nb + Ta**	**-**
		63.3	21.5	9.0	2.5	3.7	-
Grey cast iron (GJL250) substrate	[2]	**Fe**	**C**	**Si**	**Mn**	**S**	**P**
		92.35–94.4	2.9–3.65	1.8–2.9	0.5–0.7	≤0.1	≤0.3

The IN625 coatings were deposited using PCS 100 (Plasma Giken, Yorii, Japan), and the schematic is shown in Figure 1. The working gas used was N_2 and it was pressured to 60 bar and heated to 900 °C before deposition. The standoff distance from the nozzle outlet to the substrate surface was 35 mm, while the traverse scan speed was 500 mm/s. The powder feed rate was set at 65 g/min. The deposition process continued until the desired coating thickness of 1 to 1.2 mm was achieved. The DYC-8 bond coat was deposited prior to the IN625 coatings, with an average thickness of 50 μm. The spraying parameters for DYC-8 bond coat are not disclosed due to confidentiality. The coated substrate was then extracted into discs (diameter × height: 25 mm × 20 mm) and quartered into smaller samples using wire electrical discharge machining (EDM) for heat treatment (Figure 2).
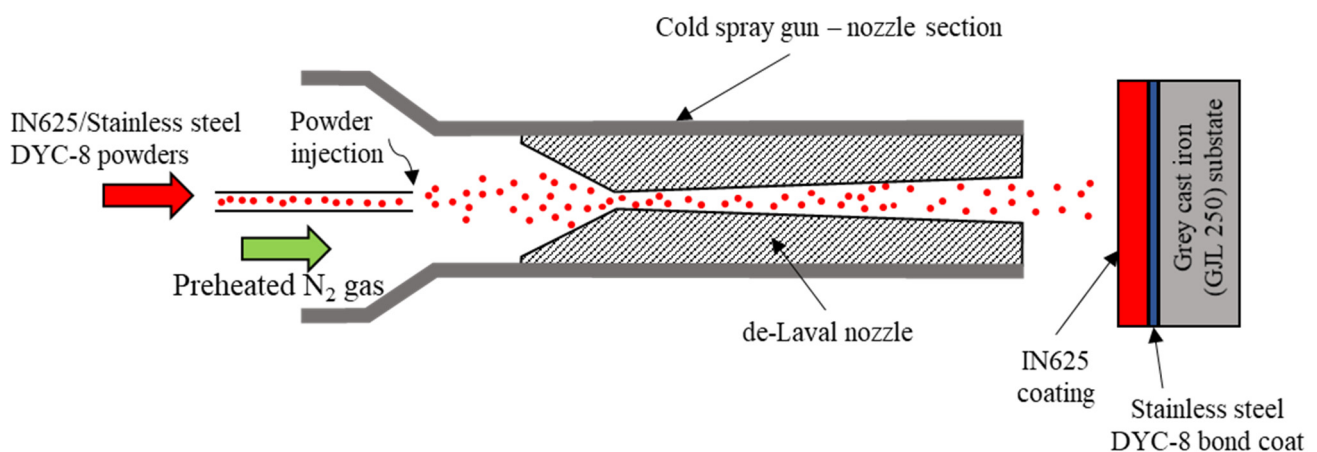

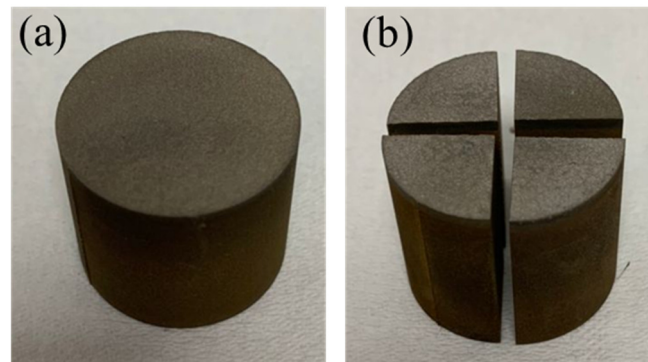**Figure 1.** Schematic of the cold spray deposition.

Figure 2. Cold sprayed sample (**a**) extracted from plate and (**b**) quartered using wire EDM process.

2.2. Heat Treatment Process

The samples were ground and degreased to remove contaminants, and subsequently heat-treated at various temperatures for different holding durations according to Table 3, using an air furnace (Lenton UAF 14, Hope, UK). The furnace was preheated to the intended temperature before inserting the samples into it. Upon completing the heat treatment, the samples were left to cool at room temperature (25 °C).

Table 3. Heat treatment of cold sprayed IN625 coating on grey cast iron (GJL250) substrate.

Sample ID (Temperature-Duration)	Temperature (°C)	Duration (h)
400-3	400	3
400-6	400	6
600-3	600	3
600-6	600	6
850-3	850	3
850-6	850	6
1050-3	1050	3
1050-6	1050	6

2.3. Characterisation

For cross-section analysis, the flat surface of the quartered samples (length × height: 12.5 mm × 20 mm) was hot mounted and polished using Struers package and steps for nickel-based superalloys.

Microstructures of the samples were observed under an optical microscope (OM, Axioskop 2 MAT, Carl Zeiss, Jena, Germany) and a scanning electron microscope (SEM JSM-5600LV) operated at 10 to 20 kV. For the porosity measurement, a series of continuous cross-section images were taken from the coating (under low magnification OM) and these images were stitched together. Subsequently, the stitched images are processed using an open-source software called ImageJ (NIH, Bethesda, MD, USA) [38]. Elemental compositions mapping/scanning of the samples were analysed using SEM-based Energy Dispersive Spectroscopy (EDS, Oxford Instrument, Oxford, UK).

The microhardness of each sample was evaluated using a Vickers microindenter (FM-300e, Future-Tech, Kawasaki, Japan), with a 300 g load. Each indentation was taken at an interval of 0.1 mm from the top of the coating to the substrate. The average coating hardness is calculated based on the sum of all coating hardness divided by the total number of indentation points in the coating.

3. Results and Discussion

3.1. Cross-Section Analysis

Figures 3 and 4 show that all the coatings are dense and do not exhibit cracking or interface delamination at different heat treatment temperatures and durations. The

porosities of IN625 coatings were between 0.25% and 3% and showed no distinct trend at different heat treatment stages. Such porosity level is comparable with other reported works of less than 3% [33,34]. The difference in porosity level for IN625 coatings deposition under similar parameters may be a result of non-uniform particle consolidation during the deposition process, due to the varying heat accumulation along the scanning paths [39]. As such, sections that experience rapid overlap scanning (less cooling), such as at the substrate ends, will accumulate more heat, which would allow the coatings to consolidate denser as compared to the middle section. For the middle section of the plate, it will have time to cool down before the next coating deposition layer. Since the initial porosity of each sample may have some fluctuation, the difference in porosity due to heat treatment is more difficult to distinguish. However, the porosity values are within a range that is acceptable in the industry.

The dense IN625 coatings are a result of the high impact energy of the particles, which produces severe plastic deformation and enhances particle cohesion. It is well established that particle bonding on the target surface occurs as a result of the occurrence of adiabatic shear instability (ASI), in which the inbound particle periphery generates jets, and the resulting shear stress leads to bonding. While a significant portion of the particle kinetic energy is converted to heat during the impact, the particles essentially deform significantly under adiabatic conditions because the heat is not dissipated within the short particle impact time (in the order of a few tens of nanoseconds) [11,38,39]. In addition, the IN625 particles conform and grip onto the bond coat surface (Figure 3d—dotted square), which proves that mechanical interlocking took place and further enhanced the bond.

Figure 3b,d,f,h,j and Figure 4b,d,f,h show that significant diffusion occurs at the interface of the coating, bond coat, and substrate with higher heat treatment temperatures and durations. The graphite flakes in the substrate dissolved at a higher percentage into the surrounding iron matrix of the grey cast iron and stainless-steel-based bond coat under the effect of heat treatment. Similarly, at the interface, the substrate/bond coat material is being diffused into the IN625 coating as the separation of the interfaces becomes less obvious and a clear diffusion gradient (darker to lighter colour contrast) is observed, for example, in Figures 3j and 4f.

The diffusion distance is measured to understand elemental movement at different stages of heat treatment. The EDS of the stainless-steel-based bond coat for the as-sprayed coating (Figure 5a) shows that it is mainly composed of 62.9% Fe, 16.4% Cr, and 10.5% Ni in terms of weightage (Figure 5b). Since the cold spray process is a relatively low-temperature process and does not alter the chemical composition of the deposited material, the bond coat chemical composition can be considered close to the original before it was deposited. This information will allow the measurement of the diffusion distance. In order to accomplish this, EDS line scans were carried out at the interface of the sample cross-section to further understand this layer (Figure 6a). Figure 6b,c shows the analysis of three primary elements (Ni, Fe, Cr) that were mainly present in the diffusion layer, and their diffusivity at different heat treatment temperatures can be used to measure the interface diffusion distance. This distance is measured from the reduction of Fe intensity to the lowest Cr intensity. The diffusion of Cr is usually further because it has higher reactivity and is more readily diffused compared to others, even at lower temperatures, according to Fick's Law [29,40]. The EDS line scan of the as-sprayed coating (Figure 6b), with a distance of 28 μm, is considered the bond coat region and does not have diffusion. Subsequent elemental composition changes will be recorded as diffusion distance.
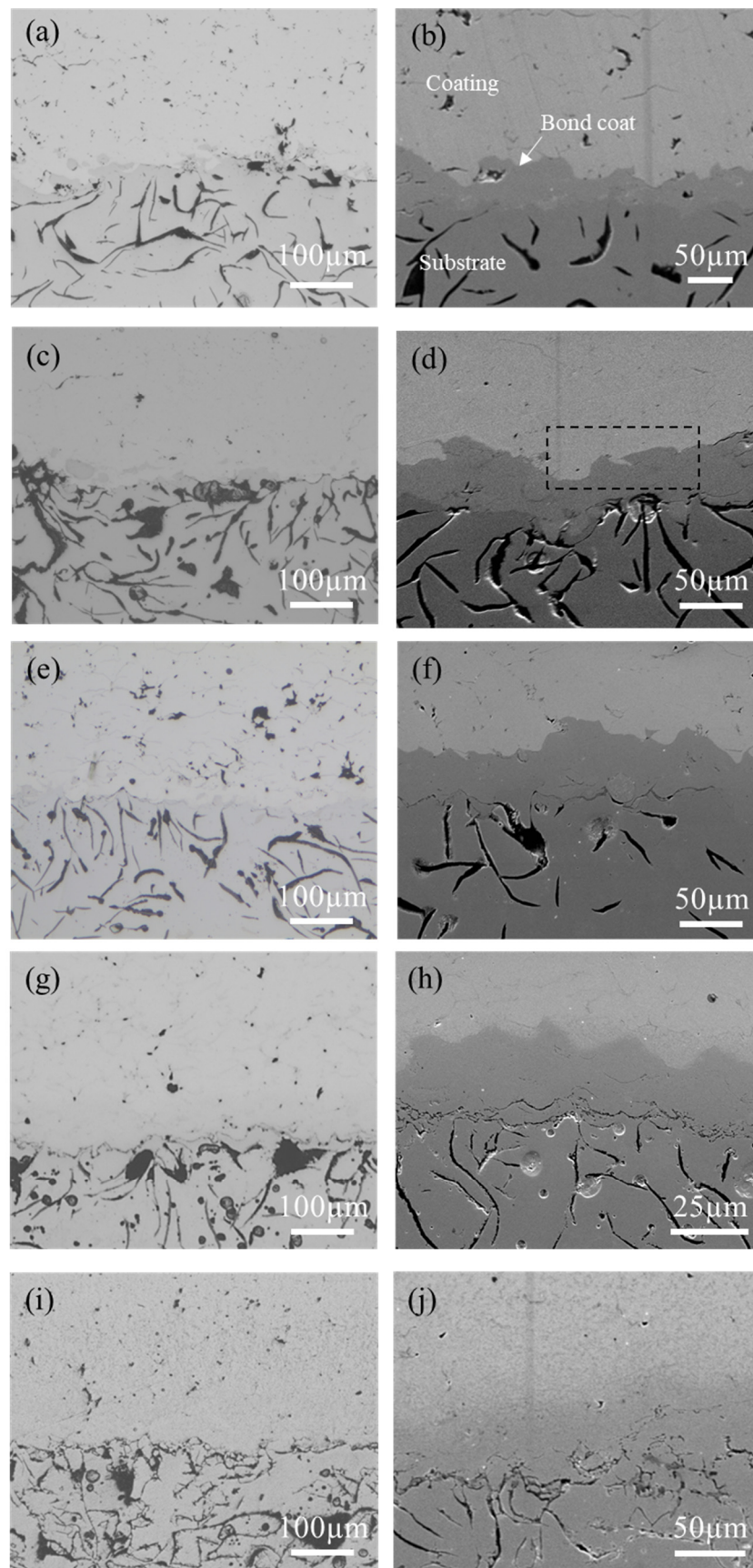
Figure 3. Optical (**a**,**c**,**e**,**g**,**i**) and SEM (**b**,**d**,**f**,**h**,**j**) micrographs of cold-sprayed IN625 coating on grey cast iron (GJL250) substrate at the interface for (**a**,**b**) as-sprayed, (**c**,**d**) 400-3, (**e**,**f**), 600-3, (**g**,**h**) 850-3 and (**i**,**j**) 1050-3. The description of the layers is shown in (**b**).
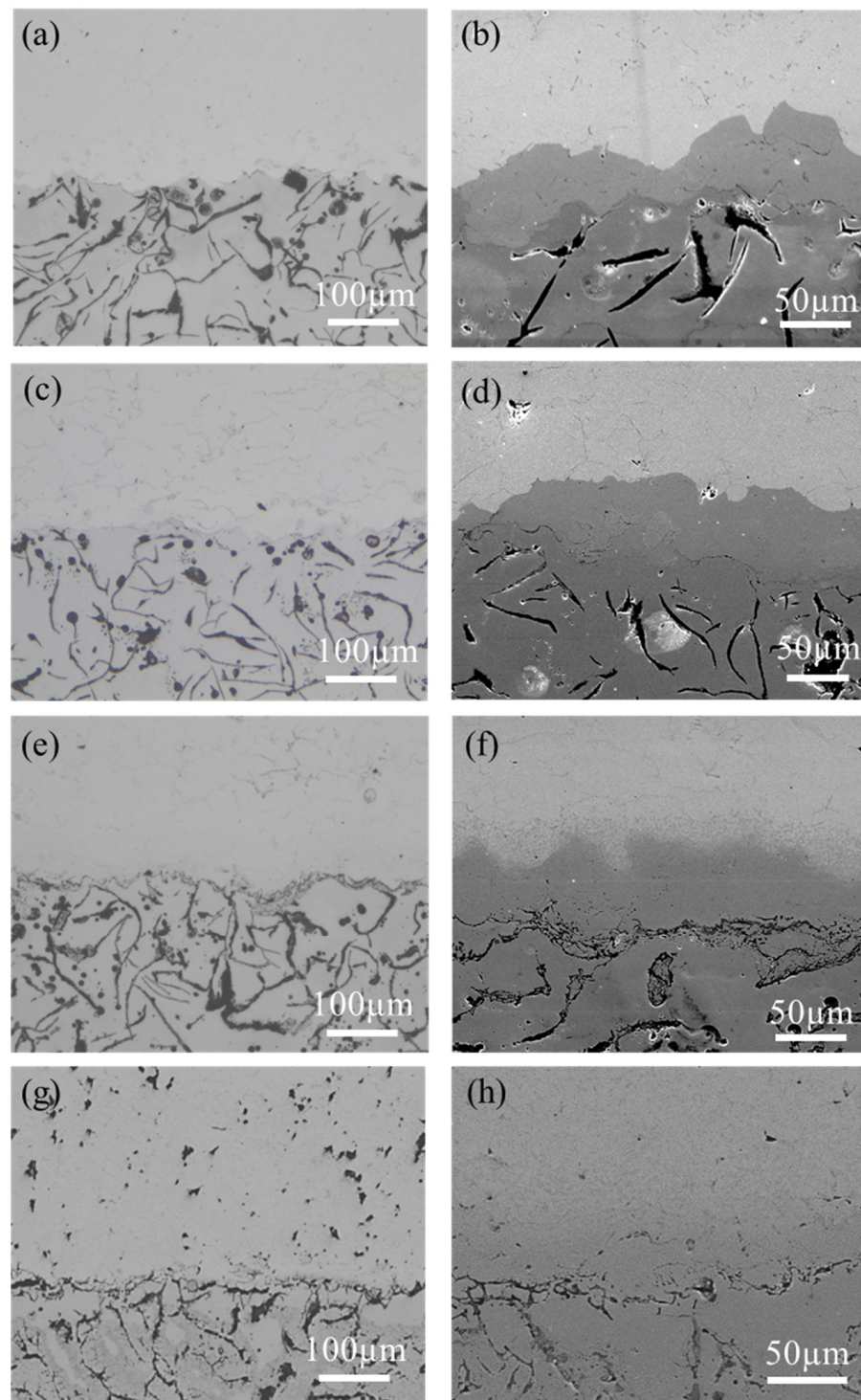
Figure 4. Optical (**a,c,e,g**) and SEM (**b,d,f,h**) micrographs of cold-sprayed IN625 coating on grey cast iron (GJL250) substrate at the interface for (**a,b**) 400-6, (**c,d**), 600-6, (**e,f**) 850-6 and (**g,h**) 1050-6. The description of the layers is shown in Figure 3b.

Figure 6d shows that the interface diffusion distance increases with both heat treatment temperatures and durations. The diffusion distance grew to 74 and 84 μm for the heat treatment temperature of 1050 °C with 3 and 6 h durations, respectively. A comparison of the interface diffusion distance between the as-sprayed and 1050-6 samples is also shown in Figure 6b,c, where the diffusion distance of the 1050-6 sample is at a greater length. This finding shows that the heat treatment process assists the bonding between the coating,

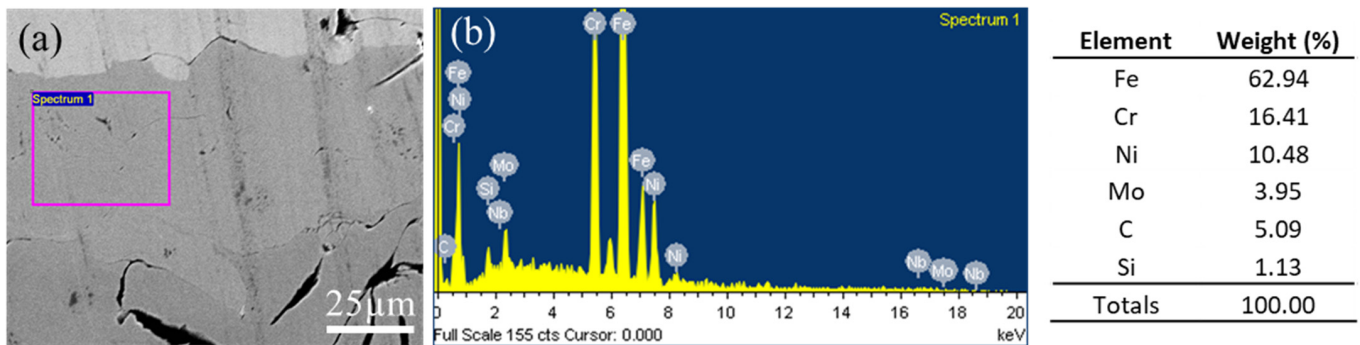bond coat and substrate, enabling the coating to be more cohesive and have better adhesion properties.

Figure 5. (**a**) EDS scanned region and (**b**) elemental composition (wt.%) of the bond coat on the as-sprayed coating.
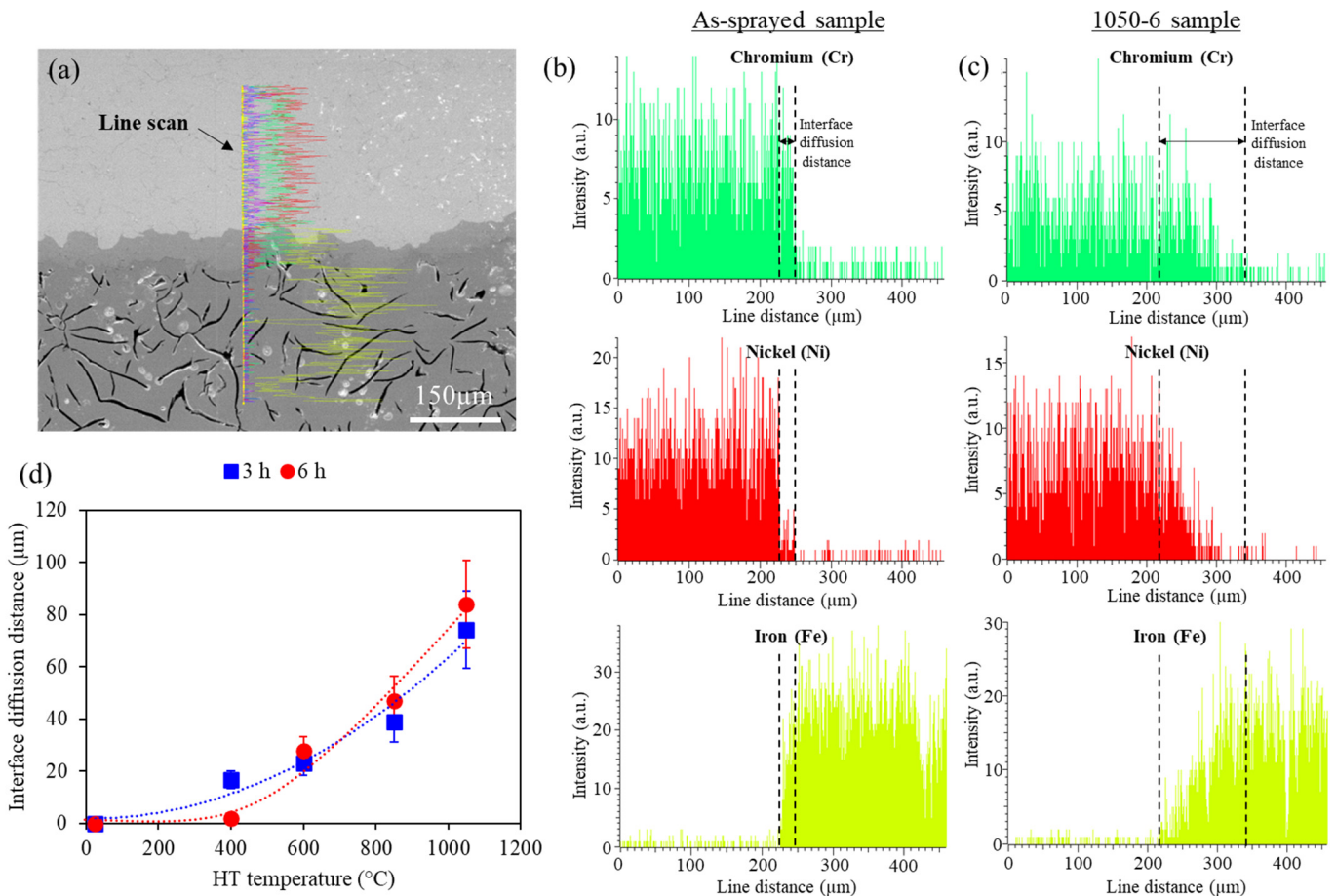

Figure 6. (**a**) SEM of 600-6 sample with the line scan location (representative sample), Elemental composition from a line scan for (**b**) as-sprayed and (**c**) 1050-6 sample, and (**d**) Interface diffusion distance at varying temperatures with 3 and 6 h hold durations.

The heat treatment of the IN625/grey cast iron sample could result in intermetallics and carbides. Based on Sukumaran et al. [41], heat treatment of IN625 in the form of bulk material would result in a single-phase austenitic with the presence of fine alloy carbides/intermetallics. The formation of carbides (MC, $M_{23}C_6$ and M_6C) and precipitates (Ni_2Cr, Mo), δ, etc., is found to occur at 625–925 °C, and dissolution of these particles occurs at 1025 °C. Heat treatment effects at the interface between IN625 and iron-based metal

(such as low alloy steel) could result in the formation of δ-phase, Ni_3Nb and carbides, i.e., $MC/M_{23}C_6$, as reported by Liu et al. [42]. The distribution of the $MC/M_{23}C_6$ phases solely at the interface region is most likely caused by grain growth during the heat treatment.

3.2. Oxidation Changes

Figure 7a shows the SEM micrographs of the IN625 coating with an EDS marked region for oxygen content analysis in the coating, to understand the oxygen penetration at different temperatures. For the samples heat-treated below 400 °C, no oxygen content is detected by EDS analysis (Figure 7b). This indicates that negligible oxides were formed in the coating because the surrounding thermal energy is below the activation energy of the coating element, which prevents the diffusion of oxygen. However, oxygen is found in the coating for 600-3, 850-3, and 1050-3 samples with concentrations of approximately 8.24%, 10.18%, and 10.54%, respectively, while the 600-6, 850-6, and 1050-6 samples were around 10.38%, 9.43%, and 20.63%, respectively (Figure 7b). This demonstrates that oxygen concentration increases with higher external temperature and duration, and when exposed to temperatures above 600 °C, the formation of oxides would occur.
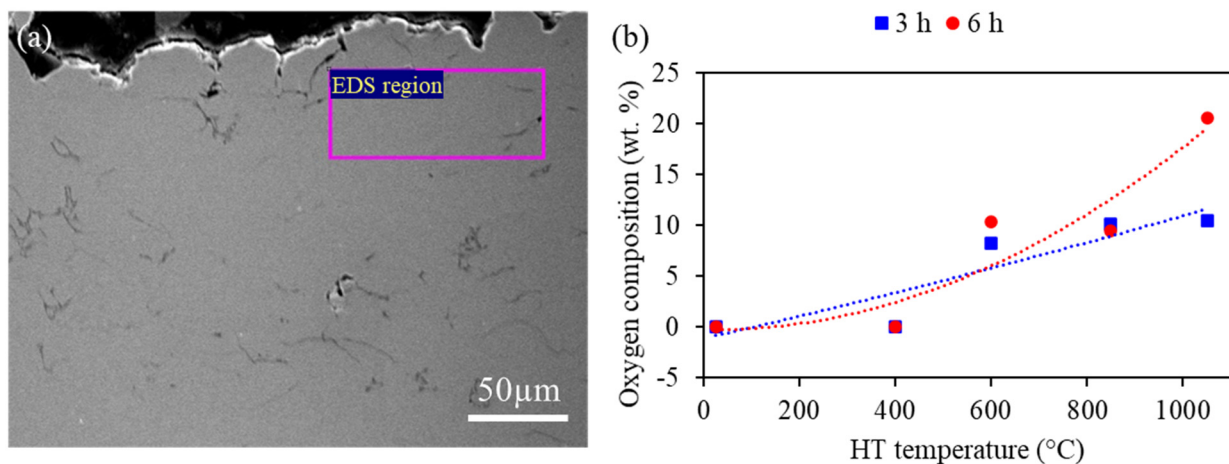

Figure 7. (**a**) SEM micrographs with EDS scanned region for 850-6 sample (representative sample), and (**b**) EDS oxygen composition of coating for different heat treatment temperatures and durations.

Figure 8a–d shows considerable oxide growth of the uncoated section of the grey cast iron substrate, as compared to their respective coated section in Figures 3g,i and 4e,g when undergoing heat treatment. Oxide is formed due to the reaction of iron and oxygen, which corrodes the grey cast iron. Figure 8e shows that the oxide growth is found to be negligible from as-sprayed condition to 600 °C heat-treated samples. From 850 °C and above, the oxide layer thickness is found to grow significantly that is from 0 to 144 and 159 μm for 850-3 and 850-6 samples, respectively, while 472 and 1085 μm for 1050-3 and 1050-6 samples, respectively. This proves that cold sprayed IN625 coating is effective in preventing degradation of grey cast iron and demonstrates that coated grey cast iron can be used in a much hotter environment.
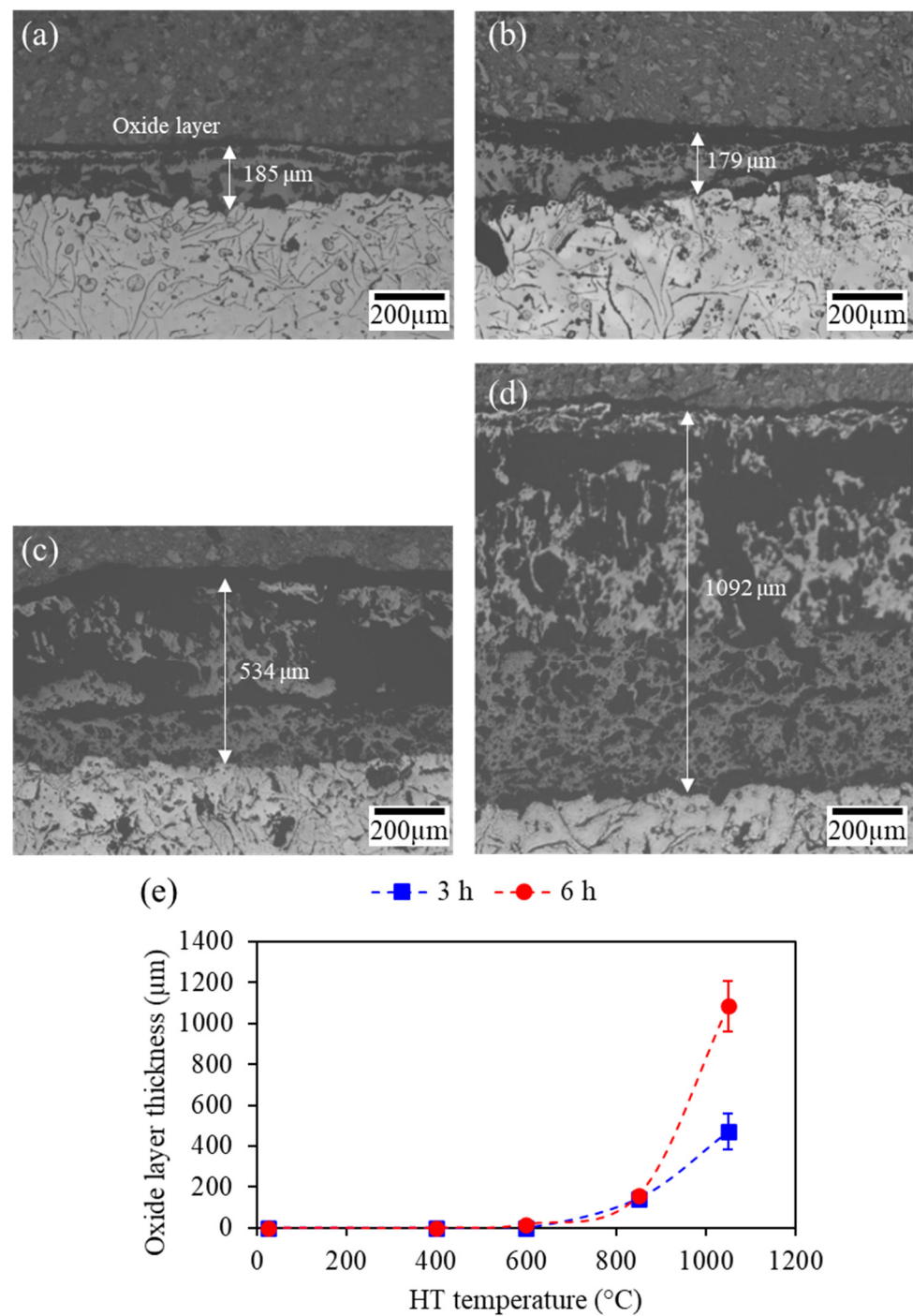
Figure 8. Oxide growth at the uncoated substrate area for (**a**) 850-3, (**b**) 850-6, (**c**) 1050-3, and (**d**) 1050-6 samples; and (**e**) Oxide layer growth as a function of heat treatment temperature and duration of the grey cast iron (GJL250) substrate.

3.3. Microhardness Profile

Microhardness of the IN625 coating on a grey cast iron substrate across different heat treatment cycles are shown in Figure 9a. The overall profile shows a distinct increment in IN625 coating microhardness from 350 to 500 HV for temperatures up to 600 °C, while the grey cast iron only has an average hardness of 145 HV. These hardness levels of the cold sprayed IN625 coatings are in a similar range to other reported works, of around 400 to 500 HV [32,34]. The increase in hardness values in the IN625 coating could be attributed to (1) the formation of recrystallized nanostructured grains [32] and (2) precipitation hardening

due to the formation of γ' [$Ni_3(Al,Ti)$] and γ'' [$Ni_3(Nb, Mo)$] phases [43]. Moreover, heat treatment could significantly promote the interfacial diffusion between different splats, thus improving the coating cohesion strength and microhardness.
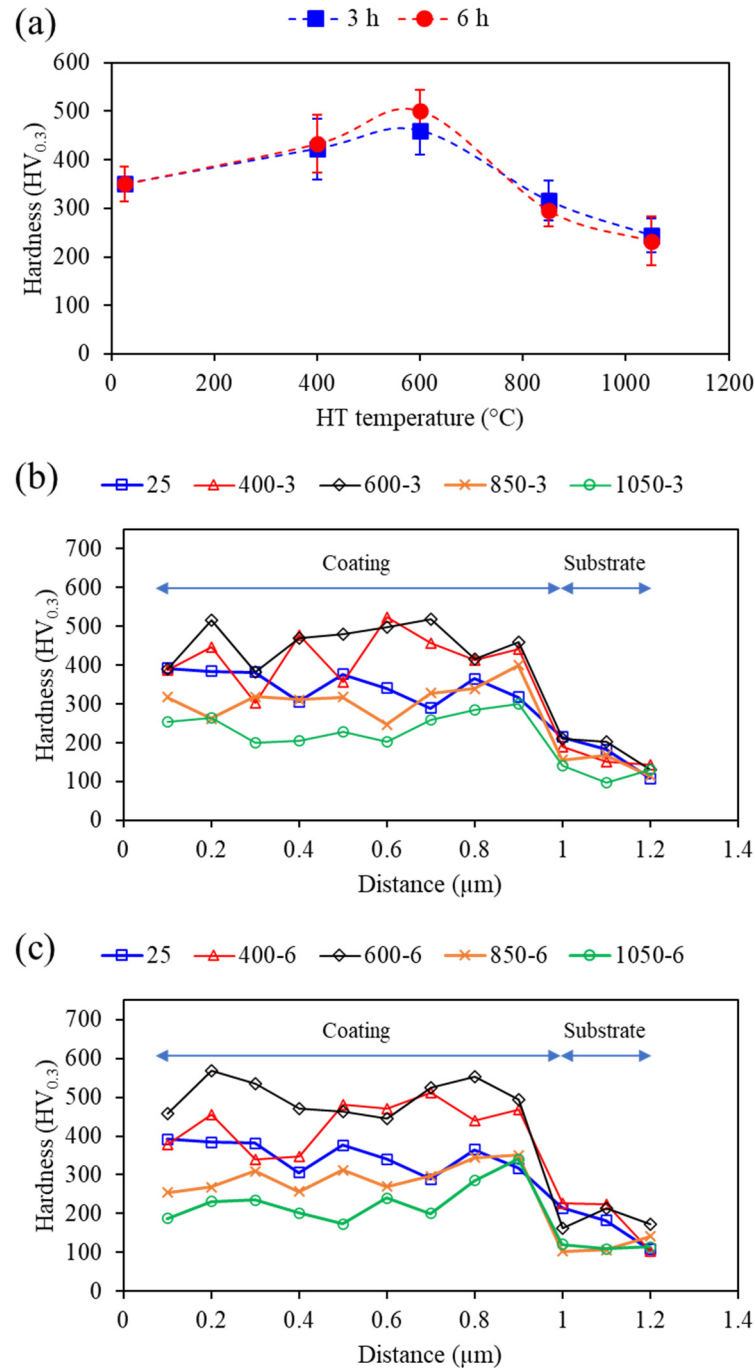

Figure 9. (**a**) Average coating hardness as a function of heat treatment temperature, and coating hardness profile across the sample cross-section for heat treated samples of (**b**) 3 h and (**c**) 6 h hold durations.

From heat treatment of 600 °C and upwards, the coating hardness decreases from 500 HV to around 300 and 240 HV for both heat treatment of 850 and 1050 °C, respectively. This phenomenon could be due to the elimination of the work-hardening effect and grain recrystallization, where stress-free grains nucleate inside old-deformed grains, replacing old-distorted grains produced by work hardening. Hence, it reverts to its original state,

which is more ductile and less strong [41]. Moreover, heat treatment at higher temperatures promotes grain growth and decreases dislocation densities within the grains, which results in a decrease in microhardness values. The hardness profile across the sample cross-section is shown in Figure 9b,c. The coating hardness of each of the samples is relatively uniform throughout their cross-section. Some fluctuations in hardness could be due to indentation at porous sites.

The hardness profile of the samples would also be affected by the residual stresses. The difference in thermal expansion of the materials will influence the residual stresses, especially on the interfaces, during the deposition process. The thermal expansion coefficients, in bulk material form, for IN625, stainless steel, and grey cast iron (GJL 250) are around $12.8 \times 10^{-6}/°C$, $17.2 \times 10^{-6}/°C$ [35], 11 to $13.0 \times 10^{-6}/°C$ [44], respectively. Furthermore, the cold spray process can introduce a combination of tensile and compressive residual stresses into the coating and substrate [45–47]. The heated gas flow and impact of the powders onto the target surfaces would raise the temperature, induce grain refinement [34] (powder and target surface), and the subsequent cooling may also give rise to thermal shrinkage [42], which will all lead to residual stress build-up.

Heat treatment of the samples would relieve the residual stresses by recrystallisation, partial dissolution of carbides [48], and reduction of porosities [46]. In a study by Shrestha et al. [46] on the heat treatment of cold sprayed IN625 coatings, it was found that the decrease in porosities during heat treatment could cause tensile stress within the microstructure. This could cancel out the compressive stress in the coating and reduce the overall residual stresses.

4. Conclusions

The cold sprayed Inconel 625 (IN625) coating on a grey cast iron (GJL250) substrate and the effects of heat treatment were systemically investigated. Based on the results obtained, the following major conclusions can be drawn:

- The IN625 coatings were found to be dense with low porosity, no cracks and delamination at the coating-substrate interface.
- The heat treatment of the samples significantly influences the atomic diffusion between the coating, bond coat, and substrate. Higher heat treatment temperatures with longer duration promote a thicker interface diffusion layer.
- Oxygen content was found to be absent in the coating at temperatures of 400 °C and below, which is an indication of a lack of activation energy. However, at temperatures above 600 °C, the oxygen concentration increases and may form oxides. Oxide growth is quite significant on the uncoated section of the grey cast iron substrate, especially for heat treatment temperatures above 850 °C, while the coated area has negligible oxide growth. Hence, cold sprayed IN625 coating is proven to be effective in preventing oxidation of grey cast iron.
- The hardness of IN625 coatings was found to have improved with heat treatment at 600 °C due to possible formation of recrystallised nanostructured grains, strengthening precipitates (γ' and γ''), and improvement of cohesion strength between different splats. However, heat treatment temperatures above 600 °C resulted in hardness reduction due to grain growth and reduction in dislocation densities within the grains.
- Cold sprayed IN625 coating onto grey cast iron is feasible, of high quality and beneficial in terms of oxidation reduction and surface enhancement (due to the higher hardness of IN625), thus providing possibilities to repair/restore grey cast iron components such as engine blocks, pump housings, etc.

Author Contributions: Conceptualization, E.L. and W.Z.; methodology, A.W.-Y.T. and N.Y.S.T.; validation, A.W.-Y.T. and K.W.; formal analysis and investigation, A.W.-Y.T., N.Y.S.T., K.W. and Y.S.C.; data curation, A.W.-Y.T.; writing—original draft preparation, A.W.-Y.T.; writing—review and editing, W.Z., W.S. and S.C.T.; visualization, A.W.-Y.T.; supervision, W.Z. and E.L.; project administration,

References

1. NovaCast Limited. Grey Iron EN-GJL-250. Available online: https://www.novacast.co.uk/alloy-specifications/grey-iron-en-gjl-250/ (accessed on 29 December 2021).
2. Gieterij Dijkkamp. Characteristics of GG25. Available online: https://www.dijkkamp.nl/en/materials/gg25-en-gjl-250/ (accessed on 29 December 2021).
3. Laouissi, A.; Yallese, M.A.; Belbah, A.; Khellaf, A.; Haddad, A. Comparative study of the performance of coated and uncoated silicon nitride (Si_3N_4) ceramics when machining EN-GJL-250 cast iron using the RSM method and 2D and 3D roughness functional parameters. *J. Braz. Soc. Mech. Sci. Eng.* **2019**, *41*, 205. [CrossRef]
4. Oerlikon Metco. Diamalloy 1005. Available online: https://mymetco.oerlikon.com/en-us/product/diamalloy1005 (accessed on 29 December 2021).
5. Shankar, V.; Rao, K.B.S.; Mannan, S. Microstructure and mechanical properties of Inconel 625 superalloy. *J. Nucl. Mater.* **2001**, *288*, 222–232. [CrossRef]
6. Sun, W.; Tan, A.W.-Y.; King, D.J.Y.; Khun, N.W.; Bhowmik, A.; Marinescu, I.; Liu, E. Tribological behavior of cold sprayed Inconel 718 coatings at room and elevated temperatures. *Surf. Coat. Technol.* **2020**, *385*, 125386. [CrossRef]
7. Gross, D. Fatigue design and safety factor for scroll compressor wraps. In *8th International Conference on Compressors and Their Systems*; Woodhead Publishing: Sawston, UK, 2013; pp. 285–300.
8. Dilthey, U. *Schweißtechnische Fertigungsverfahren 2: Verhalten der Werkstoffe beim Schweißen*; Springer: Berlin/Heidelberg, Germany, 2006.
9. The Welding Institute (TWI). Weldability of Materials—Cast Irons. Available online: https://www.twi-global.com/technical-knowledge/job-knowledge/weldability-of-materials-cast-irons-025 (accessed on 29 December 2021).
10. Gao, P.-H.; Chen, B.-Y.; Zhang, B.; Yang, Z.; Guo, Y.-C.; Li, J.-P.; Liang, M.-X.; Li, Q.-P. Preparations of iron-based alloy coatings on grey cast iron through plasma transfer arc welding. *J. Adhes. Sci. Technol.* **2021**, *36*, 833–844. [CrossRef]
11. Assadi, H.; Gärtner, F.; Stoltenhoff, T.; Kreye, H. Bonding mechanism in cold gas spraying. *Acta Mater.* **2003**, *51*, 4379–4394. [CrossRef]
12. Hassani-Gangaraj, M.; Veysset, D.; Champagne, V.K.; Nelson, K.A.; Schuh, C.A. Adiabatic shear instability is not necessary for adhesion in cold spray. *Acta Mater.* **2018**, *158*, 430–439. [CrossRef]
13. Reddy, C.D.; Zhang, Z.-Q.; Msolli, S.; Guo, J.; Sridhar, N. Impact velocity-dependent bonding mechanisms in metal cold spray. *Surf. Coat. Technol.* **2022**, *433*, 128085. [CrossRef]
14. Papyrin, A.; Kosarev, V.; Klinkov, S.; Alkhimov, A.; Fomin, V.M. *Cold Spray Technology*; Elsevier: Amsterdam, The Netherlands, 2007.
15. Dykhuizen, R.C.; Smith, M.F.; Gilmore, D.L.; Neiser, R.A.; Jiang, X.; Sampath, S. Impact of high velocity cold spray particles. *J. Therm. Spray Technol.* **1999**, *8*, 559–564. [CrossRef]
16. Vlcek, J.; Gimeno, L.; Huber, H.; Lugscheider, E. A systematic approach to material eligibility for the cold-spray process. *J. Therm. Spray Technol.* **2005**, *14*, 125–133. [CrossRef]
17. McCune, R.C.; Papyrin, A.N.; Hall, J.N.; Riggs, W.L.; Zajchowski, P.H. *An Exploration of the Cold Gas-Dynamic Spray Method for Several Materials Systems*; Advances in Thermal Spray Science and Technology; ASM International: Materials Park, OH, USA, 1995; pp. 1–5.
18. Kosarev, V.F.; Klinkov, S.V.; Alkhimov, A.P.; Papyrin, A.N. On some aspects of gas dynamics of the cold spray process. *J. Therm. Spray Technol.* **2003**, *12*, 265–281. [CrossRef]
19. Schmidt, T.; Gaertner, F.; Kreye, H. New developments in cold spray based on higher gas and particle temperatures. *J. Therm. Spray Technol.* **2006**, *15*, 488–494. [CrossRef]
20. Grujicic, M.; Zhao, C.L.; DeRosset, W.S.; Helfritch, D. Adiabatic shear instability based mechanism for particles/substrate bonding in the cold-gas dynamic-spray process. *Mater. Des.* **2004**, *25*, 681–688. [CrossRef]

21. Bae, G.; Kumar, S.; Yoon, S.; Kang, K.; Na, H.; Kim, H.J.; Lee, C. Bonding features and associated mechanisms in kinetic sprayed titanium coatings. *Acta Mater.* **2009**, *57*, 5654–5666. [CrossRef]

22. Bae, G.; Xiong, Y.; Kumar, S.; Kang, K.; Lee, C. General aspects of interface bonding in kinetic sprayed coatings. *Acta Mater.* **2008**, *56*, 4858–4868. [CrossRef]

23. Wu, K.; Chee, S.W.; Sun, W.; Tan, A.W.-Y.; Tan, S.C.; Liu, E.; Zhou, W. Inconel 713C coating by cold spray for surface enhancement of Inconel 718. *Metals* **2021**, *11*, 2048. [CrossRef]

24. Neo, R.G.; Wu, K.; Tan, S.C.; Zhou, W. Effect of spray distance and powder feed rate on particle velocity in cold spray processes. *Metals* **2022**, *12*, 75. [CrossRef]

25. Yang, Y.; Aprilia, A.; Wu, K.; Tan, S.C.; Zhou, W. Post-processing of cold sprayed CoNiCrAlY coatings on Inconel 718 by rapid induction heating. *Metals* **2022**, *12*, 396. [CrossRef]

26. Shah, Z.; Vrinceanu, N.; Rooman, M.; Deebani, W.; Shutaywi, M. Mathematical modelling of ree-eyring nanofluid using koo-kleinstreuer and cattaneo-christov models on chemically reactive AA7072-AA7075 alloys over a magnetic dipole stretching surface. *Coatings* **2022**, *12*, 391. [CrossRef]

27. Gul, T.; Nasir, S.; Islam, S.; Shah, Z.; Khan, M.A. Effective prandtl number model influences on the γAl_2O_3–H_2O and γAl_2O_3–$C_2H_6O_2$ nanofluids spray along a stretching cylinder. *Arab. J. Sci. Eng.* **2019**, *44*, 1601–1616. [CrossRef]

28. Champagne, V.; Helfritch, D. Critical Assessment 11: Structural repairs by cold spray. *Mater. Sci. Technol.* **2015**, *31*, 627–634. [CrossRef]

29. Tham, N.Y.S.; Chua, Y.S.; Wu, K.; Tan, A.W.-Y.; Tan, S.C.; Zhou, W. Effectiveness of Cold Spray Coating on Cast Iron to Prevent Oxidation. In Proceedings of the 2nd International Conference on Advanced Surface Enhancement (INCASE 2021), Singapore, 7–8 September 2021; pp. 155–158.

30. Sun, W.; Tan, A.W.Y.; Bhowmik, A.; Marinescu, J.; Huong, Y.; Liu, E. Additive manufacturing of inconel 625 superalloy parts via high pressure cold spray. In Proceedings of the 3rd International Conference on Progress in Additive Manufacturing, Nanyang Technological University, Singapore, 14–17 May 2018; pp. 14–17.

31. Chaudhuri, A.; Raghupathy, Y.; Srinivasan, D.; Suwas, S.; Srivastava, C. Microstructural evolution of cold-sprayed Inconel 625 superalloy coatings on low alloy steel substrate. *Acta Mater.* **2017**, *129*, 11–25. [CrossRef]

32. Srinivasan, D.; Chandrasekhar, V.; Amuthan, R.; Lau, Y.C.; Calla, E. Characterization of cold-sprayed IN625 and NiCr coatings. *J. Therm. Spray Technol.* **2016**, *25*, 725–744. [CrossRef]

33. Poza, P.; Múnez, C.J.; Garrido-Maneiro, M.A.; Vezzù, S.; Rech, S.; Trentin, A. Mechanical properties of Inconel 625 cold-sprayed coatings after laser remelting. Depth sensing indentation analysis. *Surf. Coat. Technol.* **2014**, *243*, 51–57. [CrossRef]

34. Wu, K.; Sun, W.; Tan, A.W.-Y.; Marinescu, I.; Liu, E.; Zhou, W. An investigation into microstructure, tribological and mechanical properties of cold sprayed Inconel 625 coatings. *Surf. Coat. Technol.* **2021**, *424*, 127660. [CrossRef]

35. Callister, W.D.; Rethwisch, D.G. *Materials Science and Engineering: An Introduction*; Wiley: New York, NY, USA, 2018; Volume 9.

36. Ltd, C.I. Alloy 625/Inconel 625. Available online: https://www.corrotherm.co.uk/grades/inconel-625 (accessed on 30 May 2022).

37. Matmatch. EN 1561 Grade GJL-250 Cast Condition. Available online: https://matmatch.com/materials/minfm36374-en-1561-grade-gjl-250-cast-condition (accessed on 30 May 2022).

38. Birt, A.M.; Champagne, V.K.; Sisson, R.D.; Apelian, D. Microstructural analysis of cold-sprayed Ti-6Al-4V at the micro- and nano-scale. *J. Therm. Spray Technol.* **2015**, *24*, 1277–1288. [CrossRef]

39. Tan, A.W.-Y.; Sun, W.; Phang, Y.P.; Dai, M.; Marinescu, I.; Dong, Z.; Liu, E. Effects of traverse scanning speed of spray nozzle on the microstructure and mechanical properties of cold-sprayed Ti6Al4V coatings. *J. Therm. Spray Technol.* **2017**, *26*, 1484–1497. [CrossRef]

40. Poirier, D.; Geiger, G. Fick's Law and Diffusivity of Materials. In *Transport Phenomena in Materials Processing*; Springer: Berlin/Heidelberg, Germany, 2016; pp. 419–461.

41. Sukumaran, A.; Gupta, R.; Kumar, V.A. Effect of heat treatment parameters on the microstructure and properties of Inconel-625 superalloy. *J. Mater. Eng. Perform.* **2017**, *26*, 3048–3057. [CrossRef]

42. Liu, H.; Tan, C.K.I.; Wei, Y.; Lim, S.H.; Lee, C.J.J. Laser-cladding and interface evolutions of inconel 625 alloy on low alloy steel substrate upon heat and chemical treatments. *Surf. Coat. Technol.* **2020**, *404*, 126684. [CrossRef]

43. Shaikh, M.A.; Ahmad, M.; Shoaib, K.A.; Akhter, J.I.; Iqbal, M. Precipitation hardening in Inconel* 625. *Mater. Sci. Technol.* **2000**, *16*, 129–132. [CrossRef]

44. VonRoll Casting ag. Grey Cast Iron. Available online: https://www.vonroll-casting.ch/en/grey-cast-iron.html (accessed on 8 May 2022).

45. Singh, R.; Schruefer, S.; Wilson, S.; Gibmeier, J.; Vassen, R. Influence of coating thickness on residual stress and adhesion-strength of cold-sprayed Inconel 718 coatings. *Surf. Coat. Technol.* **2018**, *350*, 64–73. [CrossRef]

46. Shrestha, D.; Azarmi, F.; Tangpong, X.W. Effect of Heat Treatment on Residual Stress of Cold Sprayed Nickel-based Superalloys. *J. Therm. Spray Technol.* **2021**, *31*, 197–205. [CrossRef]

47. Bhowmik, A.; Wei-Yee Tan, A.; Sun, W.; Wei, Z.; Marinescu, I.; Liu, E. On the heat-treatment induced evolution of residual stress and remarkable enhancement of adhesion strength of cold sprayed Ti–Al–4V coatings. *Results Mater.* **2020**, *7*, 100119. [CrossRef]

48. Seddighi, S.; Ostovan, F.; Shafiei, E.; Toozandehjani, M. A study on the effect of stress relief heat treatment on the microstructure and mechanical properties of dissimilar GTAW weld joints of Inconel 625 and A106 carbon steel. *Mater. Res. Express* **2019**, *6*, 086582. [CrossRef]